JOURNAL OF PROPULSION AND POWER
Vol. 26, No. 1, January–February 2010

Hybrid Particle-in-Cell Simulations of Magnetic Sail in Laboratory Experiment

Yoshihiro Kajimura*
Kyoto University, Kyoto 611-0011, Japan
Hideyuki Usui†
Kobe University, Hyogo 657-8501, Japan
Ikkoh Funaki‡
Japan Aerospace Exploration Agency, Kanagawa 229-8510, Japan
Kazuma Ueno§
Graduate University for Advanced Studies, Kanagawa 229-8510, Japan
Masanori Nunami¶
National Institute for Fusion Science, Gifu 509-5292, Japan
Iku Shinohara**
Japan Aerospace Exploration Agency, Kanagawa 229-8510, Japan
Masao Nakamura††
Osaka Prefecture University, Osaka 599-8531, Japan
and
Hiroshi Yamakawa‡‡
Kyoto University, Kyoto 611-0011, Japan

DOI: 10.2514/1.45096

Magnetic sail is a propellantless propulsion system proposed for an interplanetary space flight. The propulsive force is produced by the interaction between the magnetic field artificially generated by a hoop coil equipped with the magnetic sail and the solar wind. Three-dimensional hybrid particle-in-cell simulations are performed to elucidate the plasma flow structure around the magnetic sail and to measure the propulsive force of the magnetic sail. We report the characteristics of the magnetosphere, such as the profile of the magnetic field, the thickness of the magnetopause current layer, and the predicted thrust value obtained by simulations, which agree well with laboratory experiment when simulations are carried out by considering the ion-neutral collision effect. The hybrid particle-in-cell simulation carried out without considering the collisional effect gave a thrust value of 3.5 N, which can be applied to the thrust evaluation of the magnetic sail in a magnetosphere with size of 300 km in a collisionless interplanetary space.

Nomenclature

$\boldsymbol{B}$	=	magnetic flux density vector, T
c	=	light velocity, m/s
$\boldsymbol{E}$	=	electric field vector, V/m
$\boldsymbol{F}$	=	thrust, N
J_e	=	electron current density, J/m^2
J_i	=	ion current density, J/m^2
$\boldsymbol{J}_{\text{total}}$	=	total current density vector ($=(1/\mu_0) \times \text{rot}\mathbf{B}$), J/m^2
J_y	=	ion current density of y component, J/m^2
L	=	representative size of magnetosphere, m
M	=	magnetic moment, Tm^3
m_i	=	mass of ion, kg
m_n	=	mass of hydrogen atom, kg
$\boldsymbol{n}$	=	normal vector
n_n	=	density of hydrogen atom, m^{-3}
n_{sw}	=	density of solar wind plasma, m^{-3}
r_{Li}	=	Larmor radius of plasma (ion), m
S	=	characteristics area of magnetosphere, m^2
T_e	=	electron temperature, eV
T_i	=	ion temperature, eV
t	=	time, s
v_n	=	velocity of the hydrogen atom, m/s
v_{re}	=	relative velocity of plasma flow and neutral flow, m/s
v_{sw}	=	velocity of the solar wind plasma, m/s
α	=	degree of hydrogen ionization
δ_D	=	thickness of magnetopause, m
η	=	electric resistivity, Ωm
μ_0	=	permeability in vacuum
σ	=	momentum-transfer cross section, m^2
σ_c	=	electric conductivity, /Ωm
ω_{ci}	=	ion cyclotron frequency, 1/s

Received 23 April 2009; revision received 16 September 2009; accepted for publication 30 September 2009.

*Senior Lecturer (Industry-Government-Academia Collaboration), Division of Creative Research and Development of Humanosphere, Research Institute for Sustainable Humanosphere, Gokasyo. Also, Japan Science and Technology Agency, Core Research for Evolutional Science and Technology; kajimura@rish.kyoto-u.ac.jp. Member AIAA.

†Professor, Department of Computer Science and Systems Engineering, Graduate School of Engineering, 1-1 Rokkodaicyo.

‡Associate Professor, Institute of Space and Astronautical Science, 3-1-1 Yoshinodai. Senior Member AIAA

§Graduate Student, Department of Space and Astronautical Science, 3-1-1 Yoshinodai.

¶Assistant Professor, Department of Simulation Science, 322-6 Oroshi-cho.

**Associate Professor, Institute of Space and Astronautical Science, 3-1-1 Yoshinodai.

††Associate Professor, Department of Aerospace Engineering, 1-1 Gakuen-cho.

‡‡Professor, Division of Creative Research and Development of Humanosphere, Research Institute for Sustainable Humanosphere, Gokasyo. Senior Member AIAA.

ω_{pe} = electron plasma frequency, $1/s$
ω_{pi} = ion plasma frequency, $1/s$

I. Introduction

A HIGHLY efficient space propulsion system can help shorten the mission time to deep space. One of the promising next-generation interplanetary propulsion systems is a sail propulsion system that obtains the momentum from the solar wind that is a supersonic plasma flow. A magnetic sail, which was proposed by Zubrin and Andrews [1] in 1990, consists of a simple hoop coil and can gain a propulsive force generated by the interaction between the solar wind and artificial magnetic field that is induced by the hoop coil. The biggest advantage of the magnetic sail is that it is a propellantless system.

The artificial magnetic field blocks the solar wind, resulting in the formation of a magnetosphere. The solar wind plasma flow and the artificial magnetic field are separated by a magnetopause with a current layer. The ions entering the magnetic field are reflected back at the magnetopause, as shown in Fig. 1. The representative size of magnetosphere L (Fig. 1) is determined by the pressure balance between the dynamic pressure of the solar wind and the magnetic pressure. The thrust experienced by the magnetic sail strongly depends on the characteristics area of magnetosphere $S(=\pi L^2)$. According to the thrust generation mechanism of the magnetic sail clarified by a magnetohydrodynamic (MHD) analysis [2], to maintain the pressure balance between the magnetic field and the dynamic solar wind, an induction current shown in Fig. 1 is induced at the magnetopause. According to the Biot–Savart law, this current generates a magnetic field around the coil. The Lorentz force produced by the interaction between the coil current and the generated magnetic field acts on the coil in the form of a propulsive force.

In a recent study conducted on magnetic sails, Nishida et al. [2] demonstrated the process of momentum transfer from the solar wind to the hoop coil in a spacecraft by performing an ideal MHD simulation followed by the evaluation of the thrust on the spacecraft in MHD scale [3]. However, in the present study, the target distance of L produced by the magnetic sail is 300 km, which is not so different from the ion (hydrogen) Larmor radius r_{Li} (=100 km, shown in Fig. 1) of the solar wind at the magnetopause. For this situation, it is important to consider the ion kinetic effect, which is predominant in the interaction between the solar wind and the artificial magnetic field. Fujita [4] and Kajimura et al. [5] carried out hybrid particle-in-cell simulations, which included the effect of ion kinetics to evaluate the thrust experienced by the spacecraft in magnetospheres of various sizes. The hybrid particle-in-cell model is explained in detail in Sec. III.B. Other hybrid particle-in-cell simulations that take into account ion kinetics [6–10] have been performed to observe the interaction between the solar wind and the artificial magnetic field; however, very few published papers on this subject report a comparison between the thrust on a spacecraft observed experimentally and that observed in hybrid particle-in-cell simulations.

To gain a better understanding of the plasma flow structure around the magnetosphere with a size of $L \sim 70$ km in space, a laboratory experiment using scale-down modeling [11] was performed for a 0.1-m-size magnetosphere, which can produce a Newton-class thrust. The primary objective of this experiment was to deduce the scaling parameters such as the density, the velocity of plasma flow, and the intensity of the magnetic field, which would be used to simulate the magnetosphere in real space. Ueno et al. [12,13] recently performed a direct measurement of the propulsive force of the magnetic sail by using a thrust stand experimentally. The experimental simulator used here was the same as that used in the ground experiment previously mentioned [11]. In that experiment [12,13], scale-down parameters were used such as $L = 0.1$ m in the laboratory to reproduce the magnetosphere $L = 300$ km in space. In that experiment, the interaction between the solar wind and the artificial magnetic field around the magnetic sail was observed. Further, the profile of the magnetic flux density $\boldsymbol{B}$ was measured with a magnetic probe.

The objective of the present study is to reproduce the scale-down experiment [12,13] in the hybrid particle-in-cell simulation by using the same condition parameters as those used in the experiment and to compare the simulation results with experimental results. Furthermore, some important issues associated with the estimation of thrust on spacecrafts via laboratory experiments and those associated with the comparison between the experimental results and simulation results are elucidated through discussions on the characteristics of the magnetosphere, such as the profile of the magnetic field and the thickness of magnetopause, and the thrust measured experimentally and by the hybrid particle-in-cell simulations. Another purpose of this comparative study is to confirm the accuracy of our hybrid particle-in-cell simulation results by comparing with the experimental results. At the same time, the hybrid particle-in-cell simulation results can provide a better understanding of the plasma flow structure produced by the magnetic sail in space because of the visualization of the magnetosphere and the structure of the magnetopause ion current layer, which is not possible in the ground experiments. Finally, the expected thrust on magnetic sail with magnetosphere of size $L =$ 300 km in interplanetary space is predicted quantitatively by comparing the ground experiment conditions with the three-dimensional hybrid particle-in-cell simulation results.

II. Ground Experiment

Experimental setup of the magnetic sail, consisting of two simulators, a solar wind simulator (SWS), and a magnetic sail simulator (MSS) used in the previous ground experiment [12,13], is illustrated in Fig. 2. The coil of MSS is operated in synchronization with the activation of SWS. The SWS and MSS have a quasi-steady operating period during 0.2 msec; during this quasi-steady period, a plasma flow around the magnetic sail is observed. The parameters,

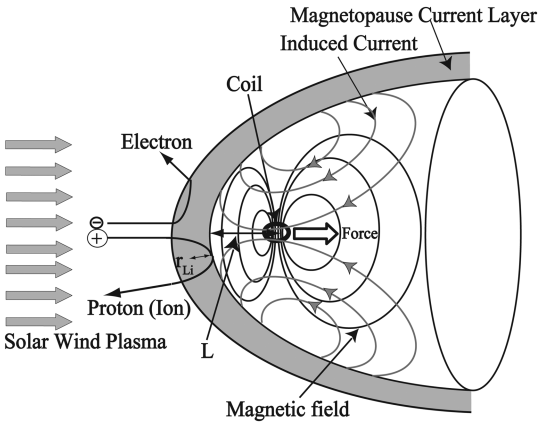

Fig. 1 Schematic diagram of interaction between solar wind plasma and magnetic field.

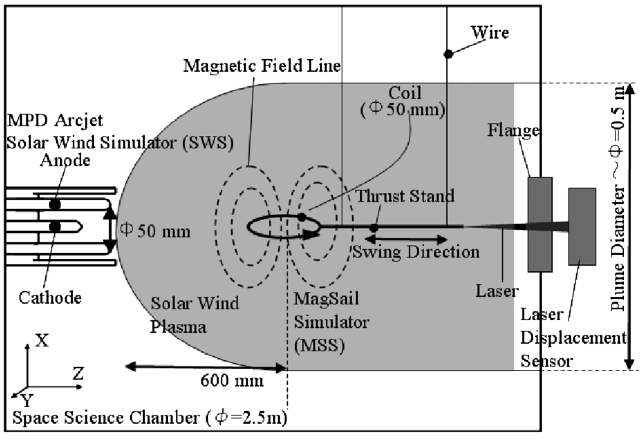

Fig. 2 Schematic diagram of experimental setup for thrust measurement of magnetic sail [12,13].

Table 1 Parameters set during ground experiment, simulations, and those in space [12,13]

Parameters	Laboratory experiment	Space	Simulation
Solar wind parameters			
Injection plasma	Hydrogen	Hydrogen	Hydrogen
Velocity u_{sw}	47 ± 28 km/s	400 km/s	47 km/s
Density n_{sw}	$1.8e+19 \pm 1.8e+18$ [m^{-3}]	$5.0e+6$ m^{-3}	$1.8e+19$ m^{-3}
Electron temperature T_e	0.84 ± 0.08 eV	10 eV	0.84 eV
Ion temperature T_i		$30 \sim 70$ eV	0.84 eV
Mass flow rate	0.4 g/s		0.4 g/s
Electric conductivity	2000 /Ωm		2000 /Ωm
Coil parameters			
Coil radius	0.025 m		0.025 m
Coil current	1800 A		1800 A
Number of turns	20		20
B field at the center of coil	0.8 T		0.8 T
Theoretical: L(magnetic cavity size)	0.11 m	300 km	0.11 m
Dimensionless parameters			
Mach number	3	8	3
Ratio of ion Lamor radius to L	0.3	0.3	0.3
Ratio of electron skin depth to L	>0.1	>0.03	>0.1
Magnetic Reynolds number Rm	<15	$1.0e+8$	<15

such as density and velocity of SWS and the intensity of coil current, are varied to design a magnetosphere with an appropriate size of L. The L as shown in Fig. 1 is given as the following Eq. (1) derived in [12]:

$$L = \left(\frac{M^2}{8\pi^2 \mu_0 n_{sw} m_i v_{sw}^2} \right)^{1/6} \tag{1}$$

In this case, it is appropriate to set the size of the magnetosphere in the scale-down modeling in the laboratory L as 0.1 m, because the parameters of the magnetoplasmadynamic (MPD) arcjet and the size of the vacuum chamber are limited. The details of the operating conditions of the plasma flow and the coil current set on the basis of the selected value of $L = 0.1$ m are summarized in Table 1. This magnetosphere of size $L = 0.1$ m in the scale-down experiment corresponds to the magnetosphere of size $L = 300$ km in real space, because both dimensionless parameters of experiment and simulation correspond well. In the present study, to match the nondimensional parameters such as Mach number M, magnetic Reynolds number R_m, the ratio of ion gyro-radii r_{Li} at the stagnation point of the magnetosphere to the representative length L of magnetosphere, ratio of electron skin depth to L, in comparison between the experiment and real space, the strength of the magnetic field generated by the coil and solar wind parameters (density, velocity, temperature) were carefully selected in the experiment. These nondimensional parameters are listed in Table 1.

In this experiment, the parameters of plasma jet such as n_{sw}, v_{sw}, and T_e were measured. The propulsive force produced in the magnetic sail simulator was also measured by a pendulum-type thrust stand. The profile of the magnetic flux density $\boldsymbol{B}$ along the direction of the plasma flow was measured with a magnetic probe; the photograph of the plasma flow around the magnetic sail was taken to observe the interaction between the magnetic field and the plasma flow, especially at the magnetopause. The numerical simulation using the 3-D hybrid particle-in-cell model is performed by using the same parameters as those measured in this laboratory experiment so as to reproduce the experimental results of the characteristics of the magnetosphere (L and profile of $\boldsymbol{B}$) and the thrust on the magnetic sail simulator.

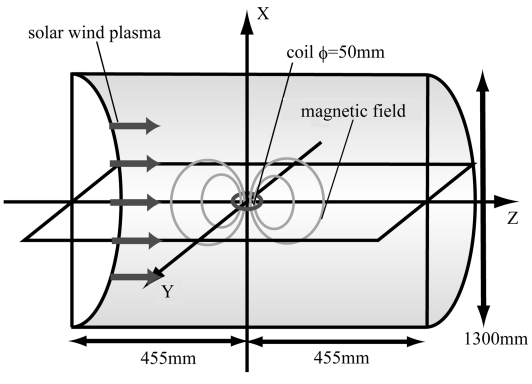

Fig. 3 Simulation model.

III. Simulation and Hybrid Particle-In-Cell Model

A. Simulation Model and Initial Parameters

The simulation model is illustrated in Fig. 3. The coil of the magnetic sail simulator is set in the origin of the simulation box. The radius of the coil and the coil current are set at the same values as those used in the laboratory experiment, which are listed in Table 1. The dipolar magnetic field calculated with the set coil parameters is set in the simulation box. The parameters associated with the plasma flow are set to the values listed in Table 1. Initially, the hydrogen ions, indicated with an arrow in Fig. 3, are injected from the side of the $-z$ boundary. The ions are injected from that region of the boundary that has a finite thickness of $v_{sw} \times dt$ and are then located randomly in that finite region. The density and velocity of the plasma flow are given by $n_{sw} = 1.8 \times 10^{19}$ m^{-3} and $v_{sw} = 47$ km/s, respectively. The velocity distribution of ion follows a Maxwellian distribution. After the plasma injection is initiated, the simulation is continued until the magnetosphere formed attains a steady state. Other simulation parameters are summarized in Tables 1 and 2.

B. Three-Dimensional Hybrid Particle-In-Cell Model

The 3-D hybrid particle-in-cell model used in the present study is based on the model proposed by Harned [14]. The hybrid particle-in-cell model treats ions as individual particles and electrons as a fluid. This approach is valid when the system behavior is dominated by ion physics. The leap-frog method [15] is adopted to solve the equation of motion of the ions. We assume a quasi-neutrality condition and set the ion charge density equal to the electron charge density. We introduce the Darwin approximation [15] in the equation of Ampere's law. To carry out stable calculations in relatively low-density plasma and strong magnetic field, we adopt the current

Table 2 Simulation parameters

dx	$0.2c/\omega_{pi}$
dt	$0.1(1/\omega_{ci})$
Number of particles per cell	25/cell
Mesh number	$100 * 100 * 70$

advance method and cyclic leapfrog method [16]. In the vacuum region, the electric field is calculated from the Laplace equation ($\nabla^2 \boldsymbol{E} = 0$) using the successive over relaxation (SOR) numerical method. A density threshold is assigned to distinguish the plasma region from the vacuum region; if the density of the plasma in a region is less than 20% of that of the injected plasma flow, then that region is considered as a vacuum region. If the density drops below a threshold in one cell, the Laplace equation is also solved by the SOR method by using the electric field at four boundary points that are calculated by the electron momentum equation. Then the digital filter is used for the electric field [17]. We checked the code against the dispersion relation of magnetized plasma [15] and found good agreement between the analytical solutions and the numerical results. During the simulation the electron temperature is kept constant. The electrical resistivity η is considered in the electron momentum equation. Generally, the electrical resistance in a plasma is approximately given by the so-called Spitzer conductivity ($\sigma_c = 1/\eta$, $\sigma_c = T_e^{3/2}/7.85\text{e}-4 = 980/\Omega\text{m}$ using $T_e = 0.84$ eV). The electric conductivity of $2000/\Omega$m listed in Table 1 is calculated using the collision frequency described in [18]. Cartesian coordinates (X, Y, Z) are adopted here and the boundary condition adopted here for the field quantities is that the spatial differences of the normal components are set to be zero at the surface of the cylindrical simulation region to avoid the numerical noise of electromagnetic field at the corner of simulation box. The $|\text{div}\boldsymbol{B}/\boldsymbol{B}|$ value in each grid, which indicates the numerical error, is confirmed to always be less than the order of 10^{-4}. The $|\text{div}\boldsymbol{B}/\boldsymbol{B}|$ value is calculated in the following way: the divergence of magnetic flux density $|\text{div}\boldsymbol{B}$ is calculated and then it is divided by that magnetic flux density $\boldsymbol{B}$ at the same grid point.

C. Collision Model

The estimated degree of hydrogen ionization α is around 0.1–0.5 for SWS–MPD in the chamber experiment [18]. The α is defined as the ratio of the n_{sw} to the density of ion and neutral gas ($n_{\text{sw}} + n_n$). Most of the hydrogen molecules H_2 dissociate into atoms (H) at a relatively high temperature of 1 eV. (at 0.5 eV, 95% dissociation). The ratio of the mean free path of H-H^+ momentum-transfer collision and the $L \sim 0.1$ m is on the order of 1. Therefore, the effect of the collision between the H and H^+ must be taken into consideration in the numerical simulation. On the other hand, in real space the ratio of the mean free path of the H-H^+ momentum-transfer collision and the representative length of the magnetosphere is 10^5. Therefore, the ion-neutral collision does not have a significant effect in interplanetary space. A Monte Carlo collision model is adopted as the elastic and momentum-transfer collision model in the particle-in-cell method [19]. The hydrogen atoms with Maxwellian distribution are assumed to be distributed throughout the simulation region. The n_n is calculated from α and n_{sw}. The flow velocity of the hydrogen atom is calculated on the basis of the mass conservation law in the plasma plume with a radius of 0.25 m as shown in Fig. 2. The momentum-transfer cross section of an elastic collision depends on the relative velocity between the hydrogen ion and atom. This cross section is calculated from the experimental data reported in [20], and this value is set to be constant throughout the simulation. A probability of the occurrence of the collision is calculated in Eq. (2)

$$P_{\text{collision}} = 1 - \exp(-n_n \sigma \cdot v_{\text{re}} \cdot \Delta t) \tag{2}$$

where σ is the momentum-transfer cross section and v_{re} is the relative velocity between the hydrogen ion and atom. The collision parameters are summarized in Table 3. Fifty percent of all collisions are treated as the charge exchange collisions described in [21]. According to this reference, the cross section of collision (H^+-Ar) is approximately $2.5\text{e}-19$ m^2. In this case, no charge exchange collisions of H^+ occur in Ar background. On the other hand, the charge exchange collisions of H^+ occur in H_2 background and the cross section of collision (H^+-H_2) is approximately $5\text{e}-19$ m^2. This increase (50% increase) of cross section causes obviously by the effect of charge exchange collision in background of same species. By using these experimental results, 50% of all collisions are treated as the charge exchange collisions in the present simulation. In the charge exchange collision, the velocities of the hydrogen ion and the atom are exchanged. Several simulations using this collision model were performed at different α from 0.1 to 0.6. For the purpose of this study, we focus on the simulation results obtained when α was 0.3 because at this $\alpha = 0.3$, the characteristics of magnetosphere and estimated thrust in the simulations are closest to the corresponding experimental results. Collision parameters are summarized in Table 3.

Table 3 Collision model parameters

Ionization ratio α	0.3
Momentum-transfer cross section ($H^+ + H$) [19]	$1.1\text{e}-19$ m^2
Neutral Density	$4.2\text{e}+19$ m^{-3}
Neutral Velocity	9.7 km/s

IV. Simulation Results

A. Characteristics of Magnetosphere

Figure 4 shows the photograph of the plasma flow taken using a shutter camera around the magnetic sail on the xz plane. There is a relatively dark region separated by the two white dotted lines, boundary 1 and boundary 2, in front of the coil. This region confirms that the plasma flow is blocked by the magnetic field produced by the coil because the dark region was not observed in experiments without the magnetic field. The distance between boundary 2 and the coil center is in good agreement with the theoretical distance L calculated from Eq. (1) using $n_{\text{sw}} = 1.8\text{e}+19$ m^{-3} and $v_{\text{sw}} = 47$ km/s.

Figure 5a shows the simulation result of the 3-D contour plot of ion density distribution averaged over the time from 5.6 μs to 9.8 μs, which corresponds to a period of 300 ion gyration time ($\omega_{\text{ci}}t$); ω_{ci} is the ion cyclotron frequency calculated from the maximum strength of the magnetic field at the coil center, which was 0.8 T. The plasma flow interacts with the magnetic field produced by the coil, resulting in the formation of the magnetosphere, which is clearly observed in Fig. 5a. Figure 5b shows the 2-D contour plot of the averaged ion density distribution on xz plane, which is an enlarged image of the dotted region shown in Fig. 5a. The coil of realistic scale is placed at the origin in Fig. 5b. The boundary is indicated by two white dotted lines at $Z = 100$–150 mm, shown in Fig. 5b. The placements of these two boundaries in Fig. 5b agree with the placements of those in Fig. 4. Also the distance between the closer boundary to the coil and the coil center agree with the theoretical distance of L.

To quantitatively compare the simulation result with the experimental result of the profile of the magnetic field along the z direction

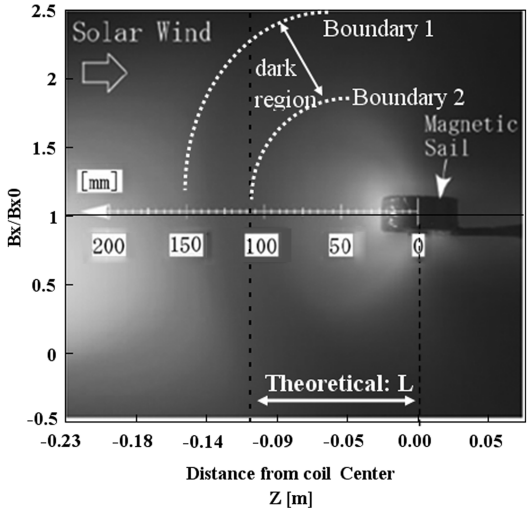

Fig. 4 Time exposure photograph of interaction between solar wind plasma and magnetic field (experimental results [12]).

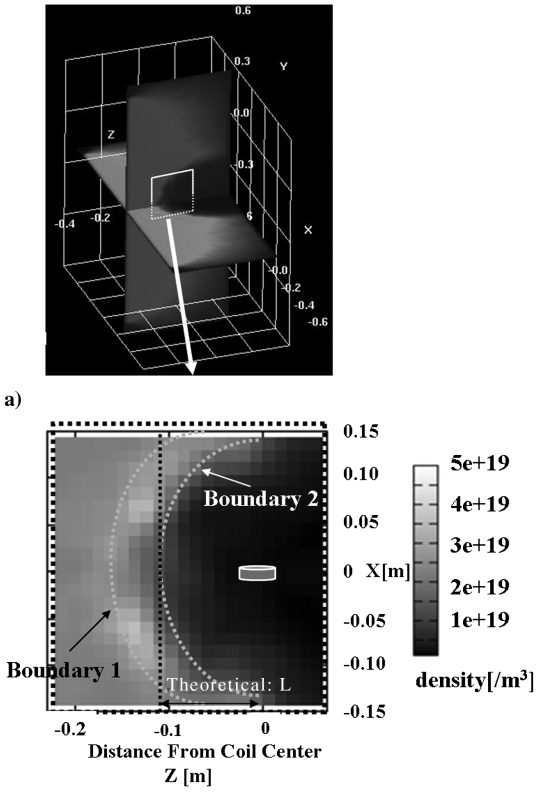

Fig. 5 a) Contour plot of ion density distribution by simulation averaged over 300 $\omega_{ci}t$ (without collision case, simulation), and b) contour plot of averaged ion density distribution on xz plane, which is the enlarged solid and dotted region of part a (without collision case, simulation).

on the coil center, the B_x/B_{x0} is plotted, as shown in Figs. 6 and 7. The vertical axis in Figs. 6 and 7 represent the magnetic flux density of the x component B_x normalized by the unperturbed magnetic flux density B_{x0} in the simulation and the experiment. The ratio B_x/B_{x0} starts to increase at the position of boundary 1 and starts to decrease at the position of boundary 2, because the unperturbed magnetosphere was compressed by the plasma flow. Figure 6 shows the profile of B_x/B_{x0} along the z direction obtained by carrying out the simulation without the collision model, indicated in black, with the experimental result indicated in gray. This profile is

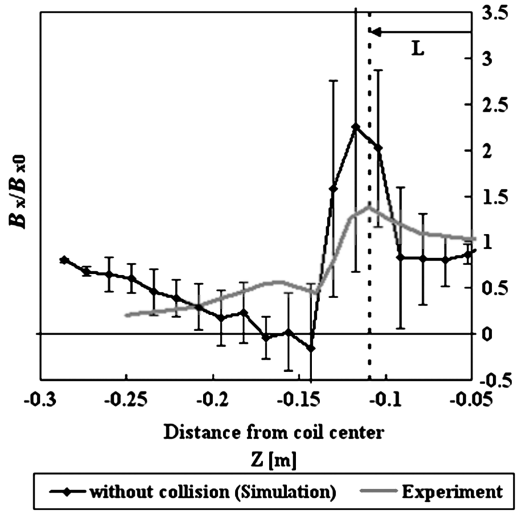

Fig. 6 Simulated B_x/B_{x0} profile along z direction obtained without collision model (gray line: experimental result, black line: simulation result).

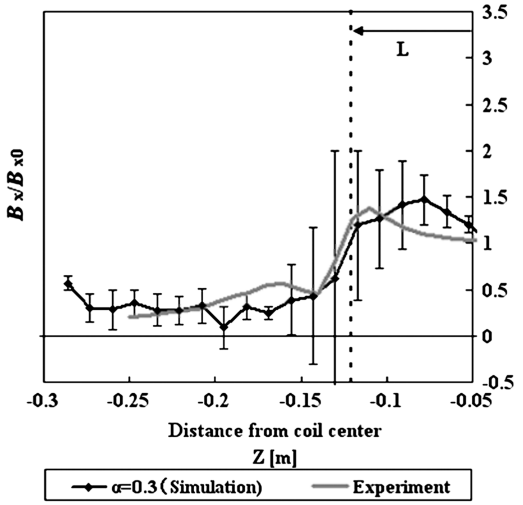

Fig. 7 Simulated B_x/B_{x0} profile along z-direction obtained with collision model (gray line represents experimental result, black line represents simulation result).

averaged over the period of 300 $\omega_{ci}t$. The dotted line in this figure indicates the theoretical distance of L from the coil center calculated by Eq. (1). The location of the maximum peak on this B_x/B_{x0} profile is in good agreement with the theoretical distance L and the position of the boundary 2 closer to the coil, as shown in Figs. 4 and 5b; however, the intensities of the maximum peak in the simulation result and the experimental result differ significantly. The error bars shown in this figure represent the standard deviations, which are the RMS deviations from the mean; these standard deviations were calculated during the same period as that over which the profile B_x/B_{x0} was averaged. The fluctuations indicated in these error bars probably include the physical phenomena and numerical noise. At the location of theoretical distance L (near boundaries 1 and 2) the fluctuations in the magnetic field would have a large amplitude because of strong interaction; consequently the value of the standard deviation would also be high in the interaction region as shown in Fig. 6.

Figure 7 shows the profile of B_x/B_{x0} along the z direction obtained when the simulation was carried out with the collision model ($\alpha = 0.3$), indicated in black, with the corresponding experimental results, indicated by the gray line. The simulation result is averaged over the period of 300 $\omega_{ci}t$. In this figure, the simulated B_x/B_{x0} profile on the magnetopause current layer is relatively diffusive compared with the collision-less case and it is in good agreement with the experimental result. In addition, the intensity of the magnetic flux density around $Z = 0.12$ m becomes close to that of the experimental result. The reason is that the impact of the plasma flow on the magnetic field decreases because the momentum of SWS-MPD's plasma flow decreases as a result of the collision between the ions and neutral atoms. This collision effect should be considered for reproducing the characteristics of experimental magnetosphere.

B. Fundamental Influences of the Ion-Neutral Collision Model

To clarify the influence to the magnetosphere given by the ion-neutral collision effect, we observe the fundamental influences of the collision model on the simulation results of the energy of plasma flow V_z, the thickness of the magnetopause current layer, and the magnitude of ion current density in a magnetopause layer by changing

Table 4 Simulation cases used to confirm fundamental influences of collision model

Base case	$\alpha = 0.3$	
	$n_n = 4.2\text{e}+19\ \text{m}^{-3}$	$v_n = 9.7$ km/s
Case 1	$n_{\text{case1}} = 0.03 \times n_n$	$v_n = 9.7$ km/s
Case 2	$n_{\text{case2}} = 0.3 \times n_n$	$v_n = 9.7$ km/s

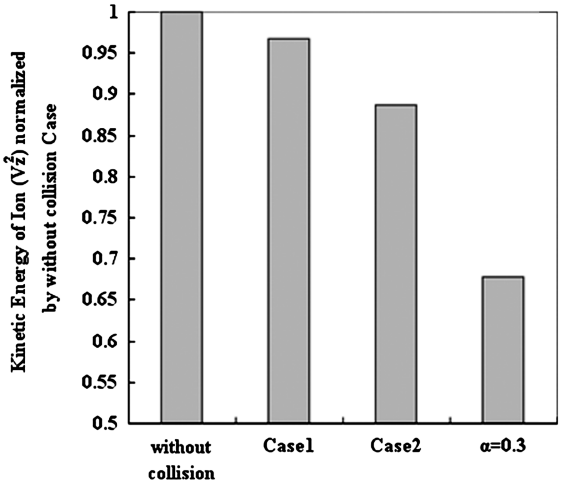

Fig. 8 Ion kinetic energy in z component in the entire simulation region.

only n_n simply based on the case of $\alpha = 0.3$. The simulation cases are listed in Table 4. The change in neutral density of 3% ($n_{\text{case1}} = 0.03n_n$) and 30% ($n_{\text{case2}} = 0.3n_n$) will change the probability of collision, as calculated in Eq. (2). Figure 8 shows the ion kinetic energy along the z component in the entire simulation region after the magnetosphere formed attained a steady state. As the collision parameter (i.e., neutral density) increases, the kinetic energy of the ion decreases due to collision effect, and the highest kinetic energy values are observed in the case of the simulation in the absence of collision model (without collision case). As a result, the decrease in the kinetic energy of plasma flow due to collision weakens the impact of the plasma flow on the magnetic field.

The ion current density at the magnetopause and the thickness of the magnetopause current layer are evaluated. The image of magnetopause and its thickness are illustrated in Fig. 1. Figure 9 shows the contour plot of the ion current density distribution as obtained by the simulation in the absence of the collision model. On interaction with the magnetic field, the hydrogen ion moves to the $-y$ direction (perpendicular to the plane in Fig. 9) due to a gyro motion, resulting in the formation of the magnetopause current layer. If r_{Li} at this magnetopause is greater than the electron skin depth c/ω_{pe}, the thickness of the ion current layer is expected to be equal to $2r_{Li}$ [22].

Figure 10 shows the profile of ion current density J_y along the z direction at $x = y = 0$ on the $A - A'$ line shown in Fig. 9. In Fig. 10, the strong ion current can be seen in the ion current layer as shown in Fig. 9. The thickness of this current layer in without collision simulation case is defined as the distance between the location P where absolute value of J_y starts to increase and the location P' where it ends to decrease ($P - P'$ shown in Fig. 10, without collision case) in the J_y distribution curve. The distance between the location at the

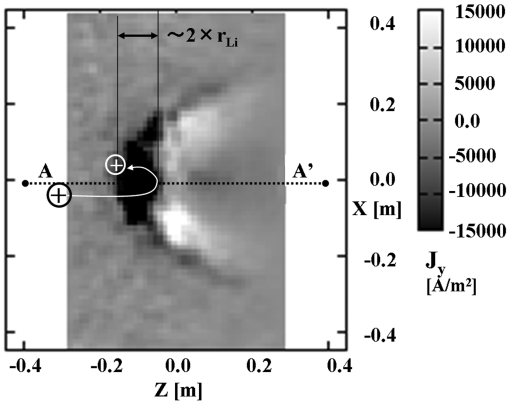

Fig. 9 Contour plot of ion current density distribution on xz plane (simulation, without collision case).

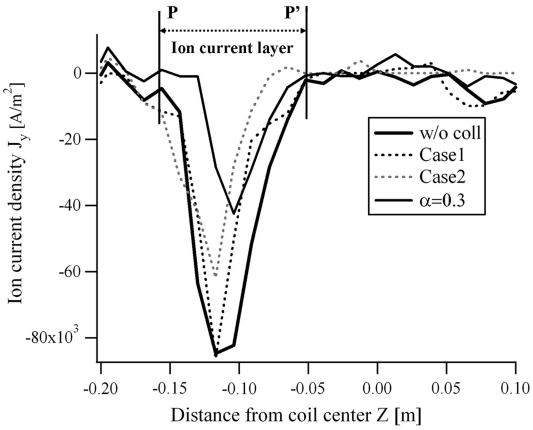

Fig. 10 Profile of the ion current J_y along z direction ($A - A'$) at $x = y = 0$ (simulation).

maximum value of absolute J_y and the coil center is in good agreement with the theoretical distance of L indicated in Fig. 5b.

From Fig. 10 it is found that with the collision model, as the neutral density increases, the thickness of this ion current layer decreases and the magnitude of the absolute J_y becomes weak. This is because a decrease in the ion momentum due to the effect of the collision weakens the impact of the plasma flow on the magnetic field. This decrease in the thickness of the ion current layer follows the same trend as that observed in the case of the decrease in the ion Larmor radius by a factor of 2, because the velocity of the ion at the magnetopause decreases due to the collision effect. The simulation results of the ion Larmor radius $r_{Li} \times 2$ and the thickness δ_D of the ion current layer $P - P'$ tend to agree with those of experimental results by considering the collision effect. The value of $r_{Li} \times 2$ for the $\alpha = 0.3$ case is 50 mm using $v_{\text{sw}} = 31$ km/s and 6.0 mT at the magnetopause in the simulation. The experimental value of $r_{Li} \times 2$ is 47 mm calculated from the experimental values, and the thickness of the current layer is 45 mm shown as the distance between boundaries 1 and 2 in Fig. 4.

C. Comparison of Thrust in the Simulation Result with That Obtained Experimentally

The thrust measured by the thrust stand in the experiment is 0.9 ± 0.5 N. This thrust value is measured as the difference between the impulse of the thrust stand when the magnetic sail simulator is operated (in the presence of the magnetic field) and the impulses when the magnetic sail simulator is not operated (in the absence of the magnetic field). This implies that the measured thrust is a purely electromagnetic Lorentz force generated on the coil.

In the present simulation, the Lorentz force generated on the coil is calculated from the simulation results with and without the collision model by using the equation as mentioned in Appendix A. Also, two other forces, the momentum conservation law and the Maxwell stress (as mentioned in Appendix A) are calculated and then we confirm that these two forces agree with the Lorentz force. In the simulation without the collision model, the thrust value is calculated to be 3.4 N

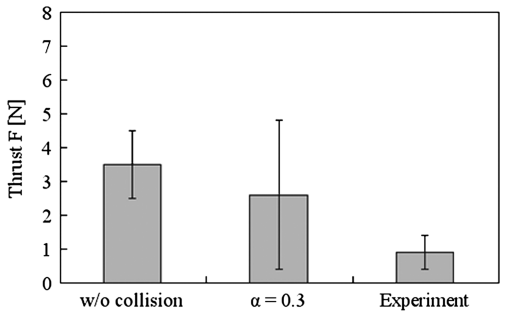

Fig. 11 Thrust estimation in simulation with/without collision model and that in experimental result.

as shown in Fig. 11. The error bars in this figure represent the standard deviation calculated during the same period as that in Figs. 6 and 7. In the case of the simulation with α of 0.3, the calculated thrust decreases to 2.5 N due to the effect of the collision; this decrease indicates a good trend for reproducing the experimental result; however, there is a significant difference between the simulation and the experimental results. This difference could be attributed to the accuracy of the simple collision model adopted in this study; other collisions such as neutral-electron collision and electron-ion collisions should be taken into consideration because the Knudsen number of these collision is less than unity. To improve the accuracy of the thrust prediction, it is important to effectively reproduce with large computational domain not only the profiles of the magnetic field and ion current but also the entire current structure considering the charge separation. For this purpose, electron dynamics need to be taken into consideration by carrying out full-particle simulations.

V. Discussion

A. Expected Thrust in Space

One of the main objectives of this research is to estimate the expected thrust of the magnetic sail in real interplanetary space. In the ground experiment, the ion-neutral collision effect can not be overlooked because the Knudsen number of H-H^+ collision is on the order of unity. The influence of this collision results in the estimation of a relatively weak thrust in the experiment as compared with the thrust observed in real interplanetary space. In fact, this is supported by the fact that the characteristics of the magnetopause and the thrust value obtained by the hybrid particle-in-cell simulation, in which the ion-neutral collision is taken into account, agree with the experimental results. However, the ion-neutral collision does not have a significant effect in interplanetary space as we mentioned in Sec. III.C; the expected thrust in the magnetic sail with the magnetosphere of size $L = 300$ km obtained in the simulation without the collision model was found to be 3.5 N. The magnetosphere generated by the magnetic sail is influenced by the solar wind and the interplanetary magnetic field (IMF) in real interplanetary space. The magnitude of the magnetic field around the magnetosphere produced by the magnetic sail is comparable to that of the IMF. Therefore, it is possible that the dynamics of this magnetosphere are predominantly controlled by magnetic reconnection, which favorably occurs under antiparallel field condition. Hence, the IMF should also be taken into consideration in the simulations carried out to estimate the thrust on a spacecraft. However, the behavior of magnetic reconnection is very complicated when both the IMF and the solar wind vary with time.

To develop magnetic sails that can be used as next-generation space propulsion systems, it is important that the small magnetosphere, which is generated by the magnetic sail having a coil with realistic size, be inflated. This can be achieved by injecting a plasma jet from a spacecraft, which has been used in the development of the magneto plasma sail (MPS) proposed by Winglee et al. [23]. Our research group plans to carry out the ground experiments on MPS for the observation of the magnetic field inflation. In addition, by means of simulations, we plan to estimate the extent of increase in the thrust that the magnetic sail can provide by using the plasma jet injection from the spacecraft for the magnetic field inflation.

B. Evaluation of Numerical Error

The hybrid particle-in-cell model treats ions as individual particles (called super particles), which are representative of a majority of particles. In the present study, one particle represents 1.5e + 12 real ions. Therefore, the influence of the motion of each super particle on the field calculation can be significant if the number of particles in each cell is not sufficient, that is, it should be more than 20/cell. In our simulations, the number of super particles is adopted 25/cell within an appropriate computational time and memory size. When the number of super particles increased from 25/cell to 125/cell, the standard deviation of the thrust and magnetic field calculation decreased to around 20–50%. On the other hand, the profile of the average magnetic field and the average thrust obtained by the numerical simulations does not change significantly if the number of ions or super particles is increased from 25/cell to 125/cell during the simulation. This means that the increase of the number of super particles can decrease the numerical fluctuation, although we can not distinguish yet because of the limited computational resources whether the fluctuation of the simulation results such as magnetic field and thrust value is caused by the physical phenomena or numerical noise. We are trying to investigate the possibility of the high-accuracy simulation by using larger computational resources to investigate the essence of the numerical fluctuation in the simulation results.

VI. Conclusions

The 3-D hybrid particle-in-cell simulation was carried out by adopting a Monte Carlo collision model because the Knudsen number of ion-neutral collision in the experiment is on the order of unity. As a result, the characteristics of a magnetosphere, such as the profile of the magnetic field, the thickness of the ion current layer, the intensity of the ion current, and the thrust value obtained in the hybrid simulation results agree well with the experimental results, when the ion-neutral collision is taken into consideration. This ion-neutral collision is one of the important issues that influences the difference between the experimental and simulation results. The result for the expected thrust calculated by the hybrid simulation without the collision model can be applied to thrust estimation of a magnetic sail in a collisionless interplanetary space. The expected thrust experienced by a magnetic sail in a magnetosphere with a size of 300 km in real interplanetary space is found to be 3.5 N.

Appendix A: Evaluation Methods of Thrust

In the experiment, the propulsive force measured by the thrust stand is treated as a purely electromagnetic Lorentz force. In the simulations, three forces are calculated to evaluate the thrust of a magnetic sail. These three forces are based on the momentum conservation law, the Maxwell stress, and the Lorentz force, respectively. The first force is derived from the momentum change in the plasma flow. The momentum change in the plasma flow is calculated by numerically integrating the momentum change of the hydrogen ions and atoms between two arbitrary times t_1 and t_2 ($\Delta t = t_2 - t_1$) described in Eq. (A1)

$$F_{\mathrm{mom}} = \frac{\sum (m_{\mathrm{sw}} \Delta v_{\mathrm{sw}} + m_n \Delta v_n)}{\Delta t} \tag{A1}$$

The second force is derived from the Maxwell stress tensor acting on the spacecraft. The electromagnetic force acting on the spacecraft can be calculated by integrating the Maxwell stress tensor over the surface area of the spacecraft. In this study, this force is denoted by F_{ms} and obtained by

$$F_{\mathrm{ms}} = \oint_{\mathrm{spacecraft}} \left(\mathbf{BB} - \frac{\mathbf{B} \cdot \mathbf{B}}{2} \right) \cdot \mathbf{n} \cdot \mathrm{d}S \tag{A2}$$

The third force is derived from the Lorentz force, which results from the induced magnetic field. The current induced by the interaction between the magnetic field and the plasma flow generates the induced magnetic field, which exerts Lorentz force on the coil fixed on the spacecraft. The electromagnetic force acting on the spacecraft is evaluated by directly calculating the Lorentz force F_L

$$F_L = \int_{\mathrm{coil}} \mathbf{J}_{\mathrm{coil}} \times \mathbf{B}_{\mathbf{i}} \, \mathrm{d}l \tag{A3}$$

where $\mathbf{J}_{\mathrm{coil}}$ is the current on the coil, as listed in Table 1, $\mathbf{B}_i$ is the induced magnetic field calculated from induced current ($\mathbf{J}_{\mathrm{total}} = \mathbf{J}_i + \mathbf{J}_e = (1/\mu_0) \times \mathrm{rot}\mathbf{B}$) by integrating the Biot–Savart law over the entire computational domain.

Acknowledgments

We gratefully acknowledge the support and advice of the members of the Magneto Plasma Sail research group in Japan. We also would like to thank Masaharu Matsumoto of the Core Research for Evolutional Science and Technology project. This study is also supported by the Japan Science and Technology Agency, Core Research for Evolutional Science and Technology. The computations were performed with the Kyoto daigaku Denpakagaku Keisanki-jikken computer system at Research Institute for Sustainable Humanosphere at Kyoto University as a part of a collaborative research project. The simulations were carried out with the support of Japan Aerospace Exploration Agency's Engineering Digital Innovation Center. This study is also partly supported by the Grant-in-Aid for Scientific Research (B) (No. 18360411) of the Japan Society for Promotion of Science.

References

[1] Zubrin, R. M., and Andrews, D. G., "Magnetic Sails and Interplanetary Travel," *Journal of Spacecraft and Rockets*, Vol. 28, No. 2, 1991, pp. 197–203. doi:10.2514/3.26230

[2] Nishida, H., Ogawa, H., Funaki, I., Fujita, K., Yamakawa, H., and Inatani, Y., "Verification of Momentum Transfer Process on Magnetic Sail Using MHD Model," AIAA, Washington, D. C., Paper 2005-4463, Jul, 2005.

[3] Nishida, H., Ogawa, H., Funaki, I., Fujita, K., Yamakawa, H., and Nakayama, Y., "Two-Dimensional Magnetohydrodynamic Simulation of a Magnetic Sail," *Journal of Spacecraft and Rockets*, Vol. 43, No. 3, 2006, pp. 667–672. doi:10.2514/1.15717

[4] Fujita, K., "Particle Simulation of Moderately Sized Magnetic Sails," *Journal of Space Technology and Science*, Vol. 20, No. 2, 2005, pp. 26–31.

[5] Kajimura, Y., Noda, K., Nakashima, H., and Funaki, I., "Feasibility Study of Magneto Plasma Sail by Using Numerical Simulation and Experiment," *Proceedings of the 45th Aerospace Sciences Meeting and Exhibit*, AIAA, Reston, VA, Paper 2007-587, Jan. 2007.

[6] Omidi, N., and Karimabadi, H., "Kinetic Simulation/Modeling of Plasma Sail," *Joint Propulsion Conference and Exhibition*, AIAA, Reston, VA, Paper 2003-5226, 2003.

[7] Khazanov, G., Delamere, P., Kabin, K., and Linde, T. J., "Fundamentals of the Plasma Sail Concept: Magnetohydrodynamic and Kinetic Studies," *Journal of Propulsion and Power*, Vol. 21, No. 5, 2005, pp. 853–861. doi:10.2514/1.3737

[8] Omidi, N., Blanco–Cano, X., Russell, C. T., and Karimabadi, H., "Dipolar Magnetospheres and their Characterization as a Function of Magnetic Moment," *Advances in Space Research*, Vol. 33, No. 11, 2004, pp. 1996–2003. doi:10.1016/j.asr.2003.08.041

[9] Tang, H., Wanga, H., Liua, C., Xianga, M., Yaoa, J., and Liu, Y., "Research Activities on Special Propulsion in BUAA," *Nuclear Physics B*, Vol. 166, 2007, pp. 286–289. doi:10.1016/j.nuclphysbps.2006.12.028

[10] Gargate, L., Bingham, R., Fonseca1, R. A., Bamford, R., Thornton, A., Gibson, K., Bradford, J., and Silva, L. O., "Hybrid Simulations of Mini-Magnetospheres in the Laboratory," *Plasma Physics and Controlled Fusion*, Vol. 50, No. 7, 2008, p. 074017. doi:10.1088/0741-3335/50/7/074017

[11] Funaki, I., Kojima, H., Yamakawa, H., Nakayama, Y., and Shimizu, Y., "Laboratory Experiment of Plasma Flow Around Magnetic Sail," *Astrophysics and Space Science*, Vol. 307, Nos. 1–3, 2007, pp. 63–68. doi:10.1007/s10509-006-9251-4

[12] Ueno, K., Kimura, T., Ayabe, T., Funaki, I., Yamakawa, H., and Horisawa, H., "Thrust Measurement of Pure Magnetic Sail," *25th International Symposium on Space Technology and Science*, Japan Society for Aeronautical and Space Sciences, Hamamatsu, Japan, 2008-b-05, 2008.

[13] Ueno, K., Funaki, I., Kimura, T., Horisawa, H., and Yamakawa, H., "Thrust Measurement of Pure Magnetic Sail Using the Parallelogram-Pendulum Method," *Journal of Propulsion and Power*, Vol. 25, No. 2, 2009, pp. 536–539. doi:10.2514/1.39211

[14] Harned, D. S., "Quasineutral Hybrid Simulation of Macroscopic Plasma Phenomena," *Journal of Computational Physics*, Vol. 47, No. 3, 1982, pp. 452–462. doi:10.1016/0021-9991(82)90094-8

[15] Horowitz, J. E., Shumaker, D. E., and Anderson, D. V., "QN3D: A Three-Dimensional Quasi-Neutral Hybrid Particle-in-Cell Code with Applications to the Tilt Mode Instability in Field Reversed Configurations," *Journal of Computational Physics*, Vol. 84, No. 2, 1989, pp. 279–310. doi:10.1016/0021-9991(89)90234-9

[16] Matthews, A. P., "Current Advance Method and Cyclic Leapfrog for 2D Multispecies Hybrid Plasma Simulations," *Journal of Computational Physics*, Vol. 112, No. 1, 1994, pp. 102–116. doi:10.1006/jcph.1994.1084

[17] Birdsall, C. K., and Langdon, A. B., *Plasma Physics via Computer Simulation*, McGraw–Hill, New York, 1985, pp. 437–441.

[18] Funaki, I., Yamakawa, H., Shimizu, Y., Nakayama, Y., Horisawa, H., Ueno, K., and Kimura, T., "Experimental Simulation of Magnetic Sails," *Joint Propulsion Conference and Exhibition*, AIAA, Reston, VA, Paper 2006-5227, July 2006.

[19] Vahedi, V., and Surendra, M., "Monte-Carlo Collision Model for Particle-in-Cell Method: Application to Argon and Oxygen Discharge," *Computational Physics Communications*, Vol. 87, 1995, pp. 179–198.

[20] Kristic, P. S., and Schultz, D. R., "Consistent Definitions for, and Relationships among, Cross Sections for Elastic Scattering of Hydrogen Ions, Atoms, and Molecules," *Physical Review A*, Vol. 60, No. 3, 1999, pp. 2118–2130. doi:10.1103/PhysRevA.60.2118

[21] Golant, V. E., Zhilinsky, A. P., and Sakharovt, I. E., *Fundamentals of Plasma Physics*, Wiley, New York, 1977, pp. 46–49, Chap. 2.6.

[22] Willis, D. M., "Structure of the Magnetopause," *Reviews of Geophysics and Space Physics*, Vol. 9, No. 4, 1971, pp. 953–985. doi:10.1029/RG009i004p00953

[23] Winglee, R. M., Slough, J., Ziemba, T., and Goodson, A., "Mini-Magnetospheric Plasma Propulsion: Tapping The Energy of the Solar Wind for Spacecraft Propulsion," *Journal of Geophysical Research*, Vol. 105, No. 21, 2000, pp. 67–77. doi:10.1029/1999JA000334

G. Spanjers
Associate Editor